



Removal of methylene blue (MB) by Bimetallic-Metal organic Framework



Naser Al Amery^{1,*}, Hussein Rasool Abid^{1,2,3}, Shaobin Wang⁴ , and Shaomin Liu¹ 

¹Chemical Engineering, WA School of Mines: Minerals, Energy and Chemical Engineering, Curtin University, Australia

²Environmental Department, Applied Medical Science, University of Karbala, Iraq

³School of Engineering, Edith Cowan University, Australia

⁴School of Chemical Engineering, University of Adelaide, Australia

ABSTRACT: In this study, three improved versions of UiO-66 were synthesised successfully: Different ratios of $\text{Ca}^{+2}/\text{Zr}^{+4}$ were used to synthesize UiO-66, UiO-66-10%Ca and UiO-66-30%Ca. These MOFs were used in batch adsorption experiments to remove different concentration of methylene blue (MB) from wastewater. When the concentration of MB was 50 ppm, UiO-66-10%Ca had the highest affinity toward MB therefore it exhibited adsorption capacity of 50.25 mg.g^{-1} . Furthermore, the MB adsorption capacity was 22.75 mg.g^{-1} and 14.84 mg.g^{-1} in UiO-66-30%Ca and UiO-66 respectively. For equilibrium study, Langmuir and Freundlich models were used to fit the experimental data. Freundlich model was the best to describe the adsorption equilibrium of MO. A kinetics study was described by pseudo first-order, pseudo second-order and intraparticle diffusion models. Pseudo second-order model demonstrated the best fitting to the experimental data. The MOFs used in this study are suggested to be attractive adsorbents to remove dyes from wastewater.

Key words: MOFs, Bimetallic, UiO-66, methylene blue, adsorption

1. INTRODUCTION

Dyes exist where there is civilisation. They are used to colour products, and employed in various industries, such as the food, paper, carpet, rubber, plastic, cosmetic, acrylic, wool, nylon, silk and textile industry [1-3].

Cationic methylene blue MB (tetramethylthionine chloride) is a basic thiazine dye as shown in Figure 1 [4]. As a basic dye, MB is not strongly hazardous, but may cause some harmful effects on humans and aquatic lives. It is also resistant to biological degradation [5].

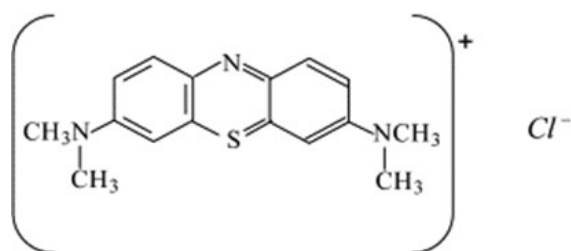


Fig. 1. Chemical structure of MB [1].

Water is a precious resource for all living creatures on earth. A significant environmental challenge is the removal of dye pollutants from fabric and textile wastewater [6]. Use of dyes to colour products consumes significant volumes of water; consequently, a substantial amount of coloured wastewater can be generated [7]. Many approaches to dye removal have been proposed to treat the industrial wastewater [8, 9]. The techniques are classified into three

main types: physical, chemical and biological treatments. These techniques include coagulation, membrane, separation process, adsorption process, filtration, softening, reverse osmosis, electrochemical processes, chemical oxidation, and aerobic and anaerobic microbial degradation [10].

The adsorption process is the simplest technique for dye removal due to its low cost, easy availability, simplicity of design, high efficiency, ease of operation [11, 12]. While activated carbon is presently believed to be the most operative adsorbent, its high cost means its production and regeneration remain uneconomical [13, 14]. This limitations of using activated carbons have led researchers to seek low-priced dye sorbents, such as coal, fly-ash, silica gel, wool waste, agricultural waste, wood waste, and clay materials [11, 15]. In recent years, research and development in the field of design and synthesis of MOFs has led to a rapid growth in practical and conceptual developments [16-21]. An extensive class of crystalline materials has become available because of metal organic framework (MOF) chemistry, which has superior characteristics such as high stability, tuneable metrics, organic functionality and porosity [16].

Its exceptional porousness means that MOFs have potentially numerous applications; their demonstrated applications in gas storage, separations, catalysis, energy

Received : October 01, 2020

Revised : November 09, 2020

Accepted : November 16, 2020

technology fuel cells, supercapacitors and catalytic conversions has made them objects of intensive study, industrial-scale production and application [22–25].

The unique characteristics of MOF-type substances that make them the focus of much worldwide research are their pore geometry and high porosity [26, 27], their central metals [28, 29], open metal sites [30, 31], functionalised linkers [32, 33] and their loading of active species [34, 35]. All these characteristics have been scientifically employed to successfully improve interactions between the sorbates and MOFs. Specifically, these characteristics distinguish MOFs from other porous material in the field of adsorption processes for the effective removal of hazardous compounds [36]. Accordingly, MOFs are superior adsorbents because of their various host–guest interactions, acid–base [37, 38], π -complexation [39], H-bonding [40, 41] and coordination with open metal sites [31, 36]. The pore size has a prime effect on the adsorption capacity of MOFs therefore exceptionally high dye uptake was demonstrated by mesoporous MOFs [42]. Very few studies were made based on bimetallic MOF [43]. UiO-66 has attractive characteristics as an adsorbent to toxic chemicals from wastewater because it has a higher hydrothermal stability among other MOFs [44]. Bimetallic-UiO-66 was recently used to significantly adsorb anionic dyes [45].

In this study, based on batch adsorption experiments, UiO-66 and UiO-66-Ca samples were used as sorbents to remove MB from an aqueous solution. Equilibrium and kinetic adsorption models were used to represent the experimental data. The equilibrium study was undertaken using Langmuir and Freundlich isotherms. The kinetics study was conducted using pseudo first-order and pseudo second-order models as well as intraparticle diffusion.

2. MATERIALS AND METHODS

2.1 Synthesis and Activation

All chemicals were supplied by Sigma-Aldrich (Australia) without further purifications.

UiO-66 was synthesised successfully using a scaled-up procedure of a previously reported method [46]. Specifically, 2.27 mmol of $ZrCl_4$ and 2.27 mmol 1,4-benzenedicarboxylic acid (BDC) were mixed with 405.38 mmol of N, N-dimethylformamide (DMF) in an autoclave and heated in a preheating oven at 393 K for 24 h. The produced UiO-66 was immersed in chloroform for 5 days to remove unreacted precursors. Then, the crystalline product was filtered and dried under vacuum at 463 K for 48 h.

UiO-66-10%Ca was synthesised by mixing $ZrCl_4$ (1.5 g) with BDC (1.1 g) in 73 mL of DMF. After mixing for 15 min, 0.15 g of $Ca(NO_3)_2 \cdot 4H_2O$ was added and followed by the addition of 2 mL of H_2O to the mixture. The solution is mixed for approximately 30 min; then transferred into a 125-mL Teflon-lined autoclave, which is tightly sealed and placed in a preheated oven at 132 °C for 1 d.

UiO-66-30%Ca was synthesised by mixing $ZrCl_4$ (1.5 g, 6.44 mmol) with BDC (1.3 g, 7.82 mmol) in 70 mL of DMF. The solution was mixed for 30 min, then $Ca(NO_3)_2 \cdot 4H_2O$ (0.45 g, 2.86 mmol, 99%; Sigma-Aldrich) was added to the

mixture. After that, 5 mL of deionised water was added into the mixture. Eventually, the mixture was transferred to a Teflon-lined autoclave which was tightly sealed and moved into a preheating oven at 430 K. The products were then filtered, dried and immersed in absolute methanol (100%, Sigma-Aldrich) for 5 d, after that it was dried and heated under vacuum at 473 K overnight before use as adsorbents.

2.2 Characterisation

The thermal stability of UiO-66, UiO66-10%Ca and UiO66-30%Ca were assessed by a thermogravimetric analysis (TGA) instrument (TGA/DSC1 STARE system; Mettler-Toledo). The samples were loaded into a pan and heated to 1173 K at a rate of 5 K/min. The air flow rate was maintained at 50 mL/min. FTIR spectra (Spectrum 100 FT-IR spectrometer, PerkinElmer, Waltham, USA) were obtained to assess the stability of the functional groups on the organic ligands. The spectra were scanned from 600 to 4000 cm^{-1} with a resolution of 4 cm^{-1} using an attenuated total reflectance technique. X-ray powder diffraction and patterns were obtained with an X-ray diffractometer (D8 Advance, Bruker AXS) using $Cu K\alpha$ radiation ($\lambda = 1.5406 \text{ \AA}$) with accelerating voltage and current of 40 kV and 40 mA respectively. Autosorb-1 (Quantachrome, instruments) was used to determine N_2 adsorption/desorption isotherms as well as the pore size and surface area of the MOFs. The samples were initially evacuated at 473 K for 24 h. Then, the sample was analysed to determine surface area, pore size and pore volume.

2.3 Adsorption Study

An aqueous stock solution of MB (1000 ppm) was prepared by dissolving MB ($C_{16}H_{18}ClN_3S$, $\geq 95\%$, Sigma-Aldrich) in deionised water. Aqueous solutions with different concentrations of MB (5–100 ppm) were prepared by successive dilution of the stock solution with water. After obtaining the UV spectra of the solutions with a spectrophotometer (UV spectrophotometer), the MB concentrations were determined using absorbance at 668 nm wavelength of the solutions. A calibration curve was obtained from the spectra of the standard solutions (5–100 ppm).

Prior to adsorption, the adsorbents were dried overnight under vacuum at 373 K. Several glass containers were cleaned, dried and filled to 20 mL with MB of different concentrations ranging from 5 to 50 ppm. An exact amount of the MOF adsorbent (20 mg) was then put in each container.

The dye solutions containing the adsorbents were mixed well with a magnetic stirrer and maintained for a period from 5 min to 24 h at 298 K. Samples for analysis were collected by a syringe filter at different sampling intervals. UV spectrometer was used to investigate the dye content in the supernatant.

Adsorbed amounts of MB by the Zr-MOFs at each time interval of time, the equilibrium and percentage removal of MB were computed according to the following equations:

$$q_t = (C_0 - C_t) \frac{V}{m} \quad (1)$$

$$q_e = (C_0 - C_e) \frac{V}{m} \quad (2)$$

$$R\% = \frac{(C_0 - C_t)}{C_0} \times 100 \quad (3)$$

Where:

q_t : the amount of MB adsorbed per unit weight of MOF at any time t (mg/g)

q_e : the amount of MB adsorbed per unit weight of MOF at equilibrium (mg/g)

C_0 : the initial concentration of the MB solution at time zero (mg/L)

C_t : the concentration of the MB solution at time t (mg/L)

C_e : the concentration of the MB solution at equilibrium (mg/L)

V : volume of the MB solution in batch adsorption process (L)

R%: percentage removal of MB [5]

m : Zr-MOF mass used in adsorption batch process (g) [1, 5, 47].

Adsorption mechanism and rate of diffusion were estimated using three kinetic models: pseudo first-order, pseudo second-order [48-50] and intraparticle diffusion model [51, 52]. The adsorbents' adsorption behaviours were simulated using the Freundlich and Langmuir adsorption isotherms [48-50, 53].

Kinetics study: Adsorption mechanism and rate of diffusion were estimated using three kinetic models: pseudo first-order, pseudo second-order [48-50] and intraparticle diffusion model [51, 52].

The nonlinear form of the Lagergren pseudo first-order kinetic equation can be written as follows [54, 55]:

$$\frac{dq}{dt} = k_1(q_e - q_t) \quad (4)$$

The linear form of the pseudo first-order kinetic equation can be expressed as follows:

$$\ln(q_e - q_t) = \ln(q_e) - k_1 t \quad (5)$$

The nonlinear form of the pseudo second-order kinetic equation can be written as follows [56]:

$$\frac{dq}{dt} = k_2(q_e - q_t)^2 \quad (6)$$

The linear form of the pseudo second-order kinetic equation can be written as follows:

$$\frac{t}{q_t} = \frac{1}{k_2 q_e^2} + \frac{1}{q_e} t \quad (7)$$

Where:

q_e : the amount of MB adsorbed per unit weight of MOF at equilibrium (mg/g)

q_t : the amount of MB adsorbed per unit weight of MOF at any time t (mg/g)

k_1 : pseudo first-order rate constant (min^{-1})

t : time (min)

k_2 : pseudo second-order rate constant (g/mg min).

A linear plot of the pseudo first-order model ($\ln[q_e - q_t]$) against time provides the values for the kinetics sorption parameters, such as rate constant (k_1), equilibrium adsorption capacity (q_e) and the linear regression coefficient (R^2). Likewise, a linear plot of the pseudo second-order model (t/q_t) against time also provides the rate constant (k_2), equilibrium adsorption capacity (q_e) and the linear regression coefficient (R^2).

As a result of the limitations of the pseudo first-order and pseudo second-order kinetic equations, the lack of an identified adsorption mechanism and the rate-limiting steps in the adsorption process, Weber and Morris established intraparticle diffusion model [117]. In general, the migration of sorbate molecules in bulk to the surface of a solid sorbent by intraparticle diffusion process is what controls the rate of most liquid/solid sorption systems. The analysis using Weber and Morris's intraparticle diffusion model is as follows [51, 52]:

$$q_t = k_p t^{1/2} + C \quad (8)$$

Where:

q_t : the amount of MB adsorbed per unit weight of MOF at any time t (mg/g)

k_p : intraparticle diffusion rate constant ($\text{mg/g min}^{0.5}$)

t : time (min)

C : constant represents the surface adsorption [57-59].

Equilibrium study: The adsorbents' adsorption behaviours were simulated using the Freundlich and Langmuir adsorption isotherms [48-50, 53].

The nonlinear form of the Langmuir isotherm can be expressed as:

$$q_e = \frac{q_m k_L C_e}{(1 + k_L C_e)} \quad (9)$$

while the linear form can be written as [60]:

$$\frac{C_e}{q_e} = \frac{1}{q_m} C_e + \frac{1}{k_L q_m} \quad (10)$$

Where:

q_m : Langmuir maximum loading capacity (mg/g)

k_L : Langmuir constant related to the energy of adsorption and affinity of binding sites (L/mg)[61]

C_e : Equilibrium concentration of dye in solution (mg/L)

q_e : Amount of dye adsorbed at equilibrium per unit mass of sorbent (mg/g).

The equilibrium experimental data were fitted using the linear form of the Langmuir isotherm equation (Equation 9). Specifically, the Langmuir parameters q_m , K_L , and R^2 were obtained from the plot of (C_e/q_e) against C_e .

The dimensionless constant separation factor, R_L , is vital to the Langmuir isotherm, and can be found in the following equation [62-65]:

$$R_L = \frac{1}{(1 + k_L C_0)} \quad (11)$$

Where C_0 is the initial concentration of adsorbate (mg/L) and K_L (L/mg) is the Langmuir constant.

The shape of the isotherm depends on R_L , because this factor indicates the adsorption process as:

Unfavourable ($R_L > 1$)

Linear ($R_L = 1$)

Favourable ($0 < R_L < 1$)

Irreversible ($R_L = 0$).

The nonlinear form of the Freundlich isotherm is written as:

$$q_e = k_F C_e^{1/n} \quad (12)$$

Whereas the linear form of the Freundlich isotherm equation can be written as [60, 66]:

$$\ln(q_e) = \ln(k_F) + \frac{1}{n} \ln(C_e) \quad (13)$$

Where K_F is the calculated Freundlich equilibrium constant ($[\text{mg/g}] [\text{L/mg}]^{1/n}$) and is an indicator of adsorption capacity, and n is a measure of the deviation from linearity of adsorption (g/L).

3. RESULTS AND DISCUSSION

3.1 Characterisation

Figure 2 shows the N_2 adsorption/desorption isotherms for UiO-66-Ca samples and UiO-66. Hysteresis in the desorption isotherm was distinguishably demonstrated by UiO-66-10%Ca which had a sharp increase in adsorption at relative pressures close to 0.999. This observation is strong evidence that the mesopore and macropore sizes were enhanced [67].

Table 1 Textural properties of the adsorbents based on N_2 adsorption/isotherm.

Adsorbents	S_{BET} (m^2g^{-1})	Pore volume (cc g^{-1})	Pore diameter (nm)
UiO-66	1585.5	0.82	1.04
UiO-66-10%Ca	918.115	1.10	2.39
UiO-66-30%Ca	557.681	0.25	0.91

In addition, Table 1 presents the textural properties of all adsorbents, according to the calculations of the N_2 adsorption isotherm. The specific surface area (S_{BET}) decreased with increasing content of a second metal. BET surface area in UiO-66 was $1585.50 \text{ m}^2\text{g}^{-1}$ and then decreased to 918.115 and $557.68 \text{ m}^2\text{g}^{-1}$ in UiO-66-10%Ca and UiO-66(Zr)-30%Ca respectively due to increasing the content of Ca in the synthesis process. The current BET values are acceptable when they compared with that in previous studies [68].

However, the pore volume and average pore size were enhanced in the MOFs with the lowest content of the second metal. The highest pore volume and pore size were seen in UiO-66-10%Ca, which were 1.10 cc.g^{-1} and 2.39 nm, respectively. The results indicate that the addition of low

concentrations of the second metal in the single-pot synthesis, followed by the activation process using the solvent exchange method, enhanced the pore volume and pore size replacing the second metal by methanol molecules which were discarded by the heating in the second stage of the activation process [69].

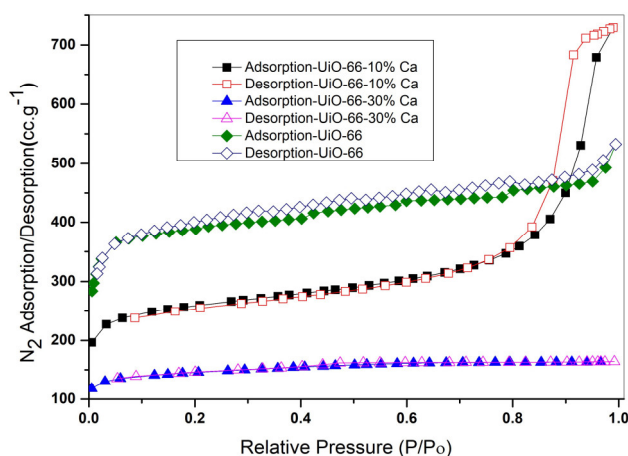


Fig. 2. N_2 adsorption/Desorption Isotherm of UiO-66 and UiO-66(Zr)-Ca.

Figure 3(a) compares the XRD patterns of UiO-66-Ca with that of UiO-66. The results demonstrate that the integrity of the structure was maintained in activated samples, which indicates that the synthesis and activation procedures succeeded reliably without suspected impurities of a metal oxide inside the pores. The XRD patterns of activated samples are similar to the XRD pattern of UiO-66 in previous studies [46, 70, 71]. The patterns of the samples after using in the adsorption experiments in Figure 3a shows that UiO-66-30% Ca demonstrated higher stability than other samples because the pattern of this sample displayed all peaks as same as those of activated samples. However, other samples were distinguished by the main characteristic peak in 2θ of 7° while other peaks were significantly reduced.

Figure 3(b) shows that the spectra of all samples, including that of UiO-66, exhibit the same vibration bands with slight deviations in the position of some peaks with increases in the content of a second metal. In addition, the peaks in the mixed-metal samples were broader than the peaks in the single-metal (Zr) sample, which indicates a difference in the dipole between ground state and excited state in the mixed-metal UiO-66 as a result of incorporating a second metal in the metal centre [72, 73]. The vibration band of $1615\text{--}1580 \text{ cm}^{-1}$ was attributed to C=C-C stretching in the aromatic ring of terephthalate salts; however, this band extended from 1590 to 1525 cm^{-1} in the mixed-metal UiO-66 [74]. Further, the bands at 1500 and 1390 cm^{-1} were attributed to the stretching vibrations of symmetric COO^- and asymmetric COO^- in coordinated organic linkers, as shown in the spectrum of UiO-66.

Moreover, the weak bands at 881 , 812 and 785 cm^{-1} were assigned to Zr-O whereas the peak at 730 cm^{-1} in the UiO-66 spectrum was assigned to the stretching vibration of C-H and out-of-plane bending of aromatic ring in the main skeleton of UiO-66; this peak was shifted to 744 cm^{-1} in the

spectra of bimetal UiO-66 [73, 75]. In addition, the band at 1017 cm^{-1} belonged to C-H stretching in the MOF.

Figure 3(c) presents the results of thermogravimetric analysis for all adsorbents in this study. All samples appear to have the same thermal stability, with structural stability at increasing temperatures up to 725 K.

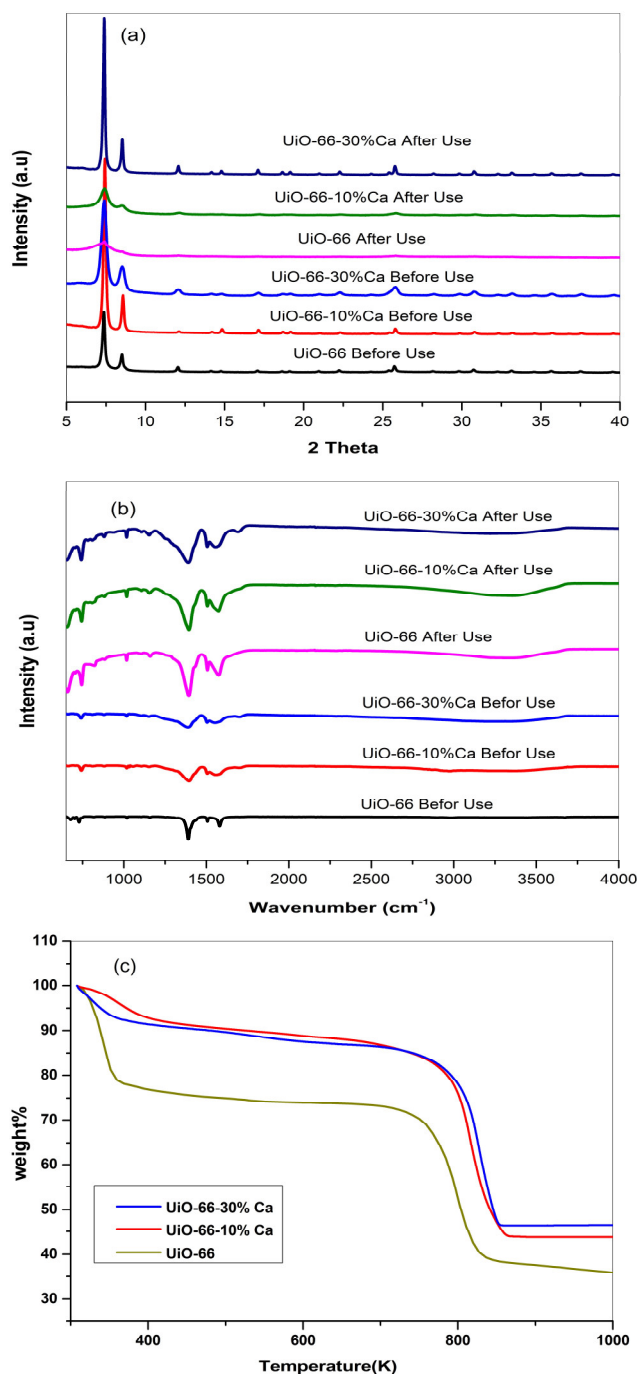


Fig. 3. Characterisation of UiO-66 samples. (a) PXRD patterns, (b) FTIR spectra and (c) TGA profiles of the UiO-66 samples.

3.2 Kinetic modelling study

Figure 4a-f describes the adsorption kinetics of MB by single-metal UiO-66 and bimetal UiO-66(Zr)-Ca. This Figure shows the amount of dye adsorbed (mg/g) on the adsorbents during different time periods (min) for various initial concentrations of MB. For all MB concentrations, MB

uptake at the commencement of the adsorption process is very rapid; after an initial period of time, it proceeds at a slower rate until the saturation is attained [76-78].

This phenomenon can be explained thus: the first available MB molecules are favourably adsorbed onto the most active sites of the single-metal and bimetal Zr-MOF, and the high initial MB uptake is possible because of the accessibility of many active sites. A longer contact time between the MOFs and MB results allows to increase the removal of MB until equilibrium adsorption capacity is reached [78]. Another explanation is that a higher initial concentration of MB provides more MB molecules and greater driving force of the aqueous phase (MB) against the solid phase (MOFs) to overcome mass-transfer resistance. This fact gives rise to increase collisions between MB molecules and active sites on the adsorbent [79, 80]. For instance, the adsorption capacity for MB onto UiO-66 at equilibrium increased from 2.151 to 14.837 mg.g^{-1} with increase in MB concentration from 5 to 50 mg.L^{-1} . Also, the adsorption capacity in UiO-66-Ca 10% and UiO-66-30%Ca was higher than that of UiO-66. It was reported that vacant metal sites in bimetallic MOFs are enhanced after removing the second metal by the solvent exchange activation [81]. Therefore, removing of Ca from UiO-66-Ca increased the active sites and consequently enhanced the adsorption capacity of MB [81].

The pseudo first-order and pseudo second-order model were employed for the adsorption of MB onto UiO-66, UiO-66-10%Ca and UiO-66-30%Ca. The linear regression correlation, R^2 , was calculated to identify the model of best fit; higher R^2 values mean a better fit for the experimental data. The results of the correlational analysis of the amount of adsorbed dye (mg/g) against contact time, for the various initial concentrations of MB (5 , 15 , 30 and 50 ppm) are shown in Figure 4. The results indicate that the amount of dye loading (q_t , [mg/g]) increases with contact time at each level of MB concentration. In addition, the amount of MB adsorbed increased with increasing in the initial MB concentration [47].

The kinetics of the adsorption process in the laboratory-based on batch experiments enables the prediction of the rate at which a pollutant is removed from bulk solutions, which informs the design of adsorption treatment plant columns [82]. However, the physical and chemical properties of the adsorbent significantly affect its adsorption kinetics, which in turn, affects the sorption mechanism. Statistics from kinetics studies of pseudo first-order and pseudo second-order kinetics model equations have been investigated for fit with contact time data [76]. Tables 2 and 3 below present their main characteristics as calculated kinetic constants (k_1 , k_2) and correlation coefficients (R^2) for $C_i = 5$, 15 , 30 and 50 ppm.

According to the R^2 values obtained, they have been consistent and closer to unity for the pseudo second-order kinetic equation than for the pseudo first-order kinetic equation. Therefore, based on R^2 values, the sorption kinetics of MB removal using single-metal and bimetal Zr-MOF were well described by the pseudo second-order kinetic equation. Further, the calculated equilibrium adsorption capacity agreed with the experimental

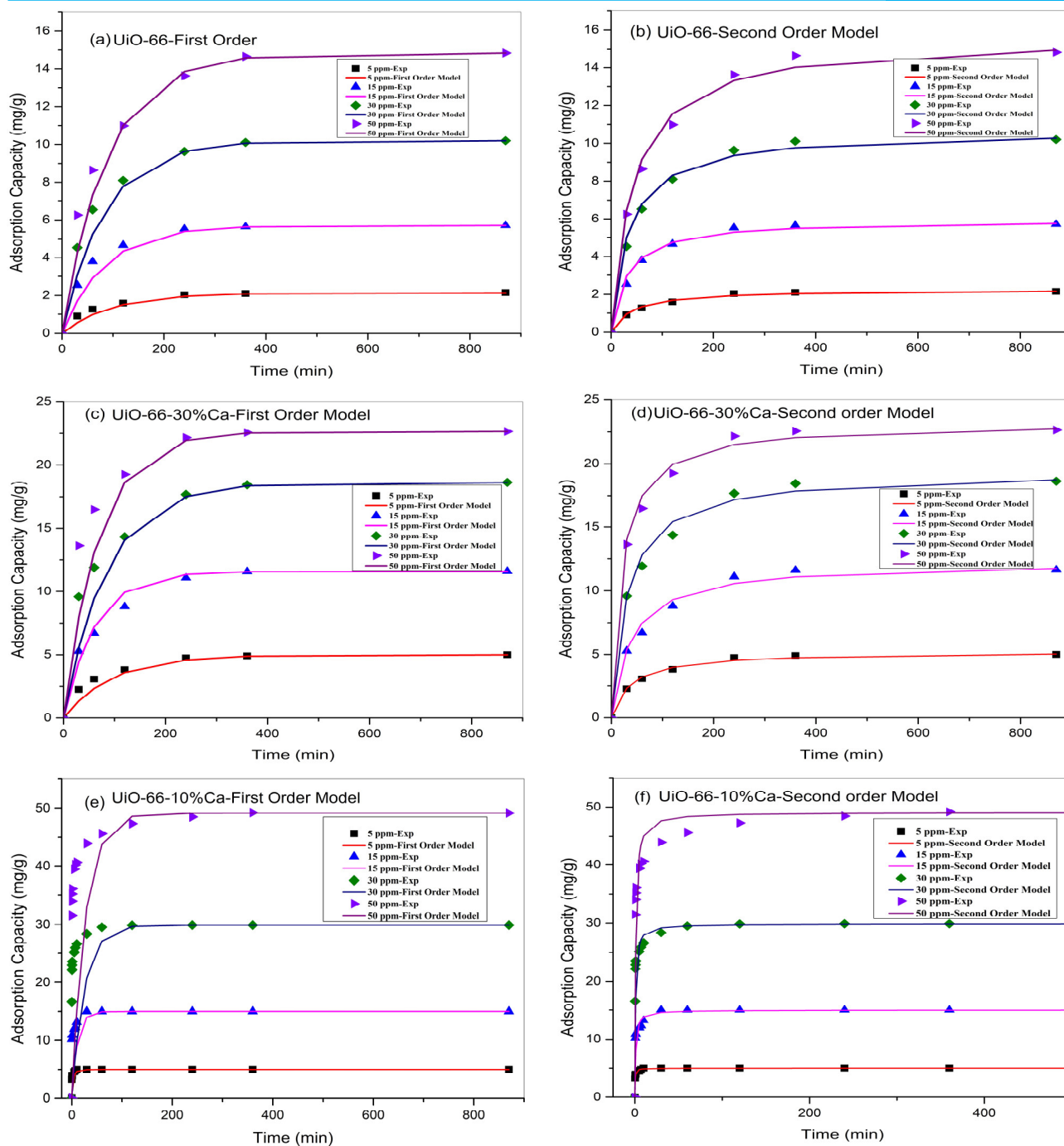


Fig. 4. Fitting of experimental data by first-order and second-order kinetic models of MB adsorption onto UiO-66 (a, b), UiO-66-30%Ca (c, d) and UiO-66-10%Ca (e, f).

equilibrium adsorption capacity, further indicating that the sorption of aqueous MB onto single-metal and bimetal Zr-MOF perfectly obeyed pseudo second-order kinetics that indicates strong interactions happened between MB and active sites in UiO-66 [83]. Specifically, the sorption of MB by single and bimetal Zr-MOFs occurred through chemisorption (the exchange or sharing of electrons between the sorbate and sorbent via covalent forces and ion exchange) [56, 83].

Based on the mechanism underlying pseudo second-order kinetics, the effects of the initial concentration on the adsorption kinetics of MB onto the three MOFs (i.e., all the sorbent systems) were similar over time. UiO-66-10%

Ca was taken to be a representative adsorbent and was used to explain the effects of the initial concentration on the rate of adsorption. Precisely, Table 2 shows that the adsorption rate constants (k_2) of Pseudo second-order model on UiO-66-10% Ca were higher than those on other adsorbents. Specifically, k_2 on UiO-66-10% Ca was 0.86348, 0.07616, 0.04628 and 0.02259 $\text{g mg}^{-1} \cdot \text{min}^{-1}$ at initial MB concentrations of 5, 15, 30 and 50 $\text{mg} \cdot \text{L}^{-1}$, respectively, signifying a decrease in adsorption rate at higher initial concentrations of MB. Reductions in the amount adsorbed at higher initial concentrations may be due to MB molecules having to enter the pores through a longer diffusion path. On the other hand, with less amounts of MB adsorbed, MB

molecules tend to be rapidly adsorbed into the open pores of MOFs, which eventually increases the adsorption rate (K_2). Table 3 shows the kinetic constant of Pseudo first-order model (K_2) and R^2 . K_1 of UiO-66-10% Ca was also higher than that of UiO-66 and UiO-66-30% Ca. For instance, it

was 0.0101, 0.2669 and 0.0105 respectively at initial concentration of 5 ppm. The lower rate constant for MB adsorption onto the UiO-66-30% was tentatively ascribed to MB diffusion into the micropores of the MOF [84].

Table 2 Calculated kinetics constant (k_2) and correlation coefficient (R^2) for $C_i = 5, 15, 30$ and 50 ppm.

Adsorbent	Adsorbate	Pseudo second-order kinetics constant k_2 (g/(mg.min))							
		5 ppm		15 ppm		30 ppm		50 ppm	
		k_2	R^2	k_2	R^2	k_2	R^2	k_2	R^2
UiO-66	MB	0.01050	0.9989	0.00546	0.9992	0.00273	0.9992	0.00147	0.999
UiO-66-10% Ca	MB	0.86348	0.9999	0.07616	0.9963	0.04628	0.9999	0.02259	0.9998
UiO-66-30% Ca	MB	0.00498	0.9991	0.00212	0.9984	0.00167	0.9992	0.00217	0.9996

Table 3 Calculated kinetics constant (k_1) and correlation coefficient (R^2) for $C_i = 5, 15, 30$ and 50 ppm.

Adsorbent	Adsorbate	Pseudo first-order kinetics constant k_1 (min ⁻¹)							
		5 ppm		15 ppm		30 ppm		50 ppm	
		k_1	R^2	k_1	R^2	k_1	R^2	k_1	R^2
UiO-66	MB	0.0101	0.9888	0.0119	0.9920	0.0120	0.9925	0.0113	0.9813
UiO-66-10% Ca	MB	0.2669	0.9716	0.0913	0.9731	0.0395	0.9886	0.0370	0.9920
UiO-66-30% Ca	MB	0.0105	0.9930	0.0161	0.9636	0.0118	0.9927	0.0144	0.9960

3.3 Intraparticle diffusion modelling study

A multistep adsorption process consists of the mass transfer of MB from the solution to the surface of single-metal and bimetal UiO-66; this transfer determines the extent of reaction throughout the whole adsorption process [85]. Adsorption process mechanism of MB onto MOFs can be arranged into the following three stages:

1. Film diffusion: the initial stage of rapid adsorption
2. Successive intraparticle diffusion: the second stage of the process during which the adsorption rate slows
3. The final stage: the adsorption attains equilibrium and lasting constant.

Film diffusion is very fast because of the rapid sorption of MB to the surface of the MOF. This stage is featured by quick surface mass transfer caused by a large differential which acts as a driving force. This stage is when the most is adsorbed by adsorbents, according to Weng et al. [86]. Such a finding establishes MOF-MB systems as entailing a fast adsorption process. Consequently, these adsorbent systems are favourable alternatives for removing cationic dyes from wastewater effluent. The second stage, intraparticle diffusion, is slower because the occupation of MB molecules on many of the available external sites in the first step slows the diffusion of MB molecules into the pore spaces of the MOF [85].

The mechanism of MB sorption on the surface of MOF was investigated using contact time data. Specifically, experimental data were fitted to the intraparticle diffusion model (Equation 13) and the outcomes interpreted by plotting q_t versus $t^{1/2}$ in Figure 5. The most important aspects of the intraparticle diffusion plot are first, the linear portion

and the intercept of the plot (c), which indicates the effects of the boundary layer on the adsorption process.

The second linear portion of the plot can be used to interpret intraparticle diffusion. The plot can be used to derive values for parameters, such as k_p (the diffusion rate), C and R^2 , as presented in Table 4. The k_p can be determined from the slope of the plot. The slope can be used to estimate the driving force of diffusion, which plays a critical role in the adsorption reaction. Experimental data analysis demonstrated that the k_p values increased from 0.0991 to 0.638 mg.g⁻¹min^{-(1/2)} with increases in the initial MB concentration from 5 to 50 mg.L⁻¹. Therefore, higher initial concentrations of MB increase the driving force and subsequently increase the MB diffusion rate. Further, increasing initial MB concentrations over a similar range led to increases in the intercept value (C) from 0.5017 to 3.8144 mg.g⁻¹, suggesting that an initial high concentration of basic dye is associated with a stronger boundary layer effect in the sorption process. In addition, an increase in the intercept value (C) can indicate the availability of MB on the boundary layer of UiO-66.

3.4 Equilibrium modelling study

Recent research has revealed that initial concentration of MB has a detrimental effect on adsorption process. Initial concentration of MB plays a role in determining removal efficiency of MB (R %) and equilibrium adsorption capacity (q_e); indeed, the initial concentration of MB has profound consequences for R% and q_e . The initial concentration of MB positively affected q_e and negatively affected R% [60, 78]. The observed decrease in MB removal (R% values of 43.03%

Table 4 Calculated kinetics constant (k_p), C and correlation coefficient (R^2) for $C_i = 5, 15, 30$ and 50 ppm.

Adsorbent	Initial concentration of MB solution (mg.L^{-1})	Adsorption mechanism			
		Intraparticle diffusion model			
		k_p ($\text{mg.g}^{-1}\text{min}^{-(1/2)}$)	C (mg.g^{-1})	R^2	
UiO-66	5	0.0991	0.5017	0.9999	
	15	0.22	2.1455	0.9918	
	30	0.3955	3.5763	0.9884	
	50	0.638	3.8144	0.9959	
UiO-66-10%Ca	5	0.4851	3.4862	0.9981	
	15	0.9352	9.927	0.9883	
	30	0.7581	23.867	0.9655	
	50	0.6585	39.364	0.9040	
UiO-66-30%Ca	5	0.218	1.3901	0.9983	
	15	0.5641	2.4216	0.9951	
	30	0.7423	6.186	0.9999	
	50	0.727	11.013	0.9928	

to 29.67%) by UiO-66 samples was representative of the adsorption process in all systems and confirmed the occupation of all accessible active sites on the UiO-66 above a certain concentration of MB. However, the increase in equilibrium adsorption capacity (q_e) from 2.15 to 14.83 mg/g can be attributed to the higher adsorption rate and the use of all available active sites on UiO-66 samples for sorption at higher concentrations of MB.

Equilibrium isotherms were examined using the Langmuir and Freundlich isotherms. The assumption of the Langmuir isotherm is monolayer coverage of sorbate over a sorbent with homogenous surface [5, 63]. It assumes that the adsorption process occurs at specific homogenous sites over the adsorbent; that is, when an MB molecule occupies a specific site, additional sorption cannot happen again at the same site. Successful implantation of the Langmuir adsorption isotherm has been undertaken to explain the adsorption of basic dyes such as MB from aqueous solutions [66].

According to Freundlich model, the favourability of adsorption can be estimated by the magnitude of the exponent ($1/n$), which predicts the feasibility of the adsorption process. The values of n must be greater than one for conditions to be favourable for an adsorption process [5, 87]. The constant n values of UiO-66, UiO-66-10%Ca and UiO-66-30%Ca have been calculated to be 1.29, 5.01 and 3.09, respectively. These values confirm the favourability of adsorption of MB onto single-metal and bimetal Zr-MOF. The results of the correlational analysis for K_F , n and the linear regression coefficient (R^2) for the plot of the linear form of the Freundlich model are presented in Table 5.

Figure 6 illustrates the experimental equilibrium data and the predicted theoretical isotherms for the adsorption of MB onto single-metal and bimetal Zr-MOFs. It is apparent, from Figure 6 and the R^2 values in Table 5, that there is

closer fit between the experimental data and Freundlich isotherm compared to that with the Langmuir isotherm, at higher values of R^2 .

Analyses and calculations of the Langmuir and Freundlich plots revealed that the values of the linear regression correlation coefficient (R^2) for the Langmuir model are 0.9889, 0.9951 and 0.9821, and for the Freundlich model 0.9979, 0.9973 and 0.9926, for UiO-66, UiO-66-10%Ca and UiO-66-30%Ca, respectively.

Further, Freundlich constants (K_F) related to the bonding energy of MB molecules with single-metal and bimetal Zr-MOFs were greater than Langmuir constants which were related to the affinity of MB molecules to single-metal and bimetal Zr-MOF in all cases. As a result, the adsorption of MB onto single-metal and bimetal Zr-MOF occurred as multilayer adsorption on a heterogeneous surface. The calculated maximum monolayer adsorption capacity (q_m) of Zr-MOF for MB is 50.25 mg/g for UiO-66-10%Ca, a relatively satisfactory adsorption capacity (see Table 4). According to Langmuir isotherm, the calculated results for the separation factor (R_L) are (0.89–0.44), (0.005–0.0005) and (0.28–0.03) for UiO-66, UiO-66-10%Ca and UiO-66-30%Ca, respectively. R_L values for the sorption of MB onto single-metal and bimetal UiO-66 are in the range of $0 < R_L < 1$, indicating that the adsorption was favourable. Further, higher initial MB concentrations in the adsorption process can make it irreversible [88].

Table 6 lists the maximum adsorption capacity (q_m) of the UiO-66 adsorbents in this study for MB, relative to those reported in the literature for different adsorbents of MB. The performance of UiO-66 in MB removal is relatively effective by comparison.

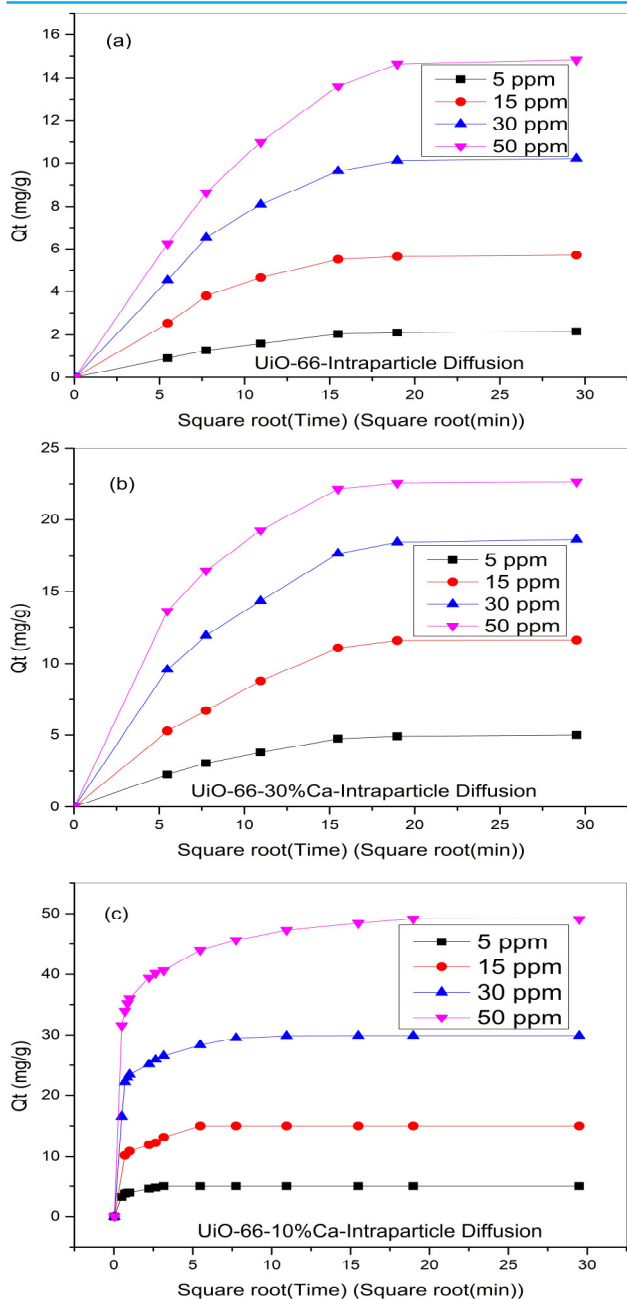


Fig. 5. Fitting of experimental data using intraparticle diffusion models of MB adsorption onto UiO-66 (a), UiO-66-30%Ca (b) and UiO-66-10%Ca (c).

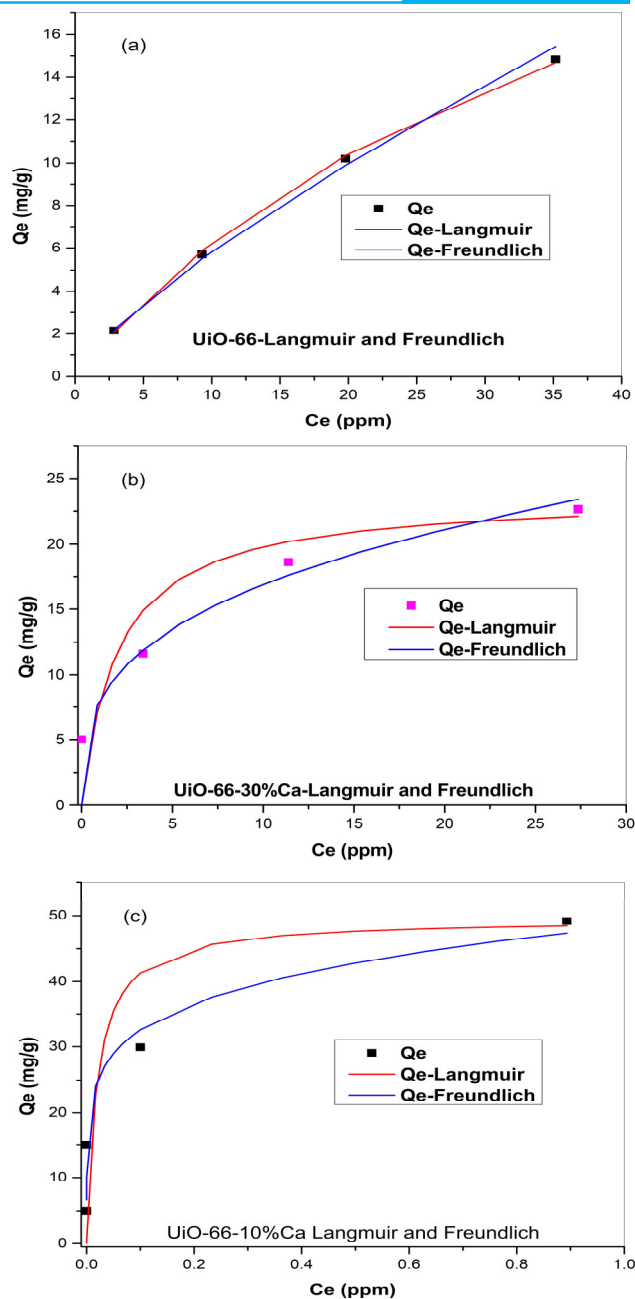


Fig. 6. Fitting of experimental data using Langmuir and Freundlich models of MB adsorption onto UiO-66 (a), UiO-66-30%Ca (b) and UiO-66-10%Ca (c).

Table 5 Calculated equilibrium constants (k_L , k_F , q_m , n and correlation coefficient (R^2)) of MB adsorption onto UiO-66, UiO-66-30%Ca and UiO-66-10%Ca for $C_i = 5, 15, 30$ and 50 ppm.

Adsorbent	Adsorption isotherm model	Parameter	Value	R^2
UiO-66	Langmuir	q_m (mg/g)	31.74	0.9889
		K_L (L/mg)	0.02447	
	Freundlich	K_F ([mg/g] [L/mg] ^{1/n})	0.98157	0.9979
		n (g/L)	1.2918	
UiO-66-10%Ca	Langmuir	q_m (mg/g)	50.2512	0.9951
		K_L (L/mg)	39.8	
	Freundlich	K_F ([mg/g] [L/mg] ^{1/n})	47.9855	0.9973
		n (g/L)	5.0150	
UiO-66-30%Ca	Langmuir	q_m (mg/g)	23.7529	0.9821
		K_L (L/mg)	0.4982	
	Freundlich	K_F ([mg/g] [L/mg] ^{1/n})	8.0164	0.9926
		n (g/L)	3.0911	

Table 6 Comparison of monolayer equilibrium capacity for methylene blue onto different adsorbents.

Adsorbent	q_m (mg/g)	Reference
Untreated coffee husks	90.1	[89]
Sewage sludge from agrifood industry wastewater treatment plant	86.957	[90]
Raw date pits	80.29	[91]
Calcined pure clay	56.31	[92]
UiO-66-10%Ca	50.25	This study
UiO-66-30%Ca	23.75	This study
UiO-66	14.52	This study
Luffa cylindrica fibres	47	[57]
Carbon nanotubes	46.2	[93]
Rice husk	40.59	[94]
Garden grass	31.4	[95]
Raw clay	27.49	[92]
Jute processing waste	22.47	[96]
Fe (III)/Cr (III) hydroxide	22.8	[60]
Banana peel	20.8	[97]
Orange peel	18.6	[97]
Activated date pits (T = 900 °C)	17.27	[91]
Fly-ash	13.42	[98]
Calcined raw clay	13.44	[92]
Activated date pits (T = 500 °C)	12.94	[91]
Zeolite	12.7	[99]
Clay	6.3	[100]
Fly-ash	1.3	[99]

4. CONCLUSION

The main goal of the current study was to assess the adsorption capacity of MB in UiO-66, UiO-66-10%Ca and UiO-66-30%Ca. The Zr-MOFs were prepared according to a single pot solvothermal methods with a modification using trace additives of Ca. Compared with the UiO-66 without the modification; the textural properties of the modified UiO-66 were enriched while their performances were enhanced to remove MB from wastewater. The kinetics of MB sorption onto UiO-66, UiO-66-10% Ca and UiO-66-30% Ca were fitted by the pseudo first and second-order models. The second model offered the best fit for the experimental data for all systems studied. The mechanism of MB sorption onto the surface of MOFs was investigated using contact time data. Specifically, the fitting of experimental data to the intraparticle diffusion model identified three stages in the sorption process.

Langmuir and Freundlich plot analyses and calculations revealed that the values of the linear regression correlation coefficient (R^2) for the Freundlich model were greater than those for the Langmuir model, for UiO-66, UiO-66-10%Ca and UiO-66-30%Ca. As a result, the adsorption of MB onto single-metal and bimetal Zr-MOFs was considered to occur as multilayer adsorption on a heterogeneous surface.

Langmuir maximum loading capacity (q_m) was compared with other reported adsorbents in previous studies. The values of the separation factor (R_L) indicated that the adsorption was a favourable process. Using the

Freundlich linear model, constant n values for UiO-66, UiO-66-10%Ca, and UiO-66-30%Ca were found to be more than one (i.e., $n > 1$). These values confirm the favourability of MB adsorption onto single-metal and bimetal Zr-MOF. This study can suggest the bimetallic UiO-66 as an attractive adsorbent to remove dyes from wastewater.

AUTHOR INFORMATION

Corresponding Author

*Email : naser.alamery@postgrad.curtin.edu.au

ORCID

Shaobin Wang : 0000-0002-1751-9162

Shaomin Liu : 0000-0001-5019-5182

REFERENCES

- [1] Almeida CAP, Debacher NA, Downs AJ, Cottet L, Mello CAD. Removal of methylene blue from colored effluents by adsorption on montmorillonite clay. *Journal of Colloid and Interface Science* 2009;332(1):46-53.
- [2] Bhattacharyya KG, Sharma A. Kinetics and thermodynamics of methylene blue adsorption on neem (*Azadirachta indica*) leaf powder. *Dyes and pigments* 2005;65(1):51-9.
- [3] Tunç Ö, Tanacı H, Aksu Z. Potential use of cotton plant wastes for the removal of Remazol Black B reactive dye. *Journal of Hazardous Materials* 2009;163(1):187-98.

- [4] Albert M, Lessin MS, Gilchrist BF. Methylene blue: dangerous dye for neonates. *Journal of Pediatric Surgery* 2003;38(8):1244-5.
- [5] Hameed BH. Spent tea leaves: A new non-conventional and low-cost adsorbent for removal of basic dye from aqueous solutions. *Journal of Hazardous Materials* 2009;161(2):753-9.
- [6] Abdelrahman EA, Hegazey R, El-Azabawy RE. Efficient removal of methylene blue dye from aqueous media using Fe/Si, Cr/Si, Ni/Si, and Zn/Si amorphous novel adsorbents. *Journal of Materials Research and Technology* 2019;8(6):5301-13.
- [7] Rafatullah M, Sulaiman O, Hashim R, Ahmad A. Adsorption of methylene blue on low-cost adsorbents: A review. *Journal of Hazardous Materials* 2010;177(1):70-80.
- [8] Gupta VK, Suhas, Ali I, Saini VK. Removal of Rhodamine B, Fast Green, and Methylene Blue from Wastewater Using Red Mud, an Aluminum Industry Waste. *Industrial & Engineering Chemistry Research* 2004;43(7):1740-7.
- [9] Robinson T, McMullan G, Marchant R, Nigam P. Remediation of dyes in textile effluent: a critical review on current treatment technologies with a proposed alternative. *Bioresource Technology* 2001;77(3):247-55.
- [10] Wang S, Zhu Z. Characterisation and environmental application of an Australian natural zeolite for basic dye removal from aqueous solution. *Journal of hazardous materials* 2006;136(3):946-52.
- [11] Bulut Y, Aydın H. A kinetics and thermodynamics study of methylene blue adsorption on wheat shells. *Desalination* 2006;194(1):259-67.
- [12] Meshko V, Markovska L, Mincheva M, Rodrigues AE. Adsorption of basic dyes on granular activated carbon and natural zeolite. *Water Research* 2001;35(14):3357-66.
- [13] Wang S, Zhu ZH. Characterisation and environmental application of an Australian natural zeolite for basic dye removal from aqueous solution. *Journal of Hazardous Materials* 2006;136(3):946-52.
- [14] Wang S, Boyjoo Y, Choueib A, Zhu ZH. Removal of dyes from aqueous solution using fly ash and red mud. *Water Research* 2005;39(1):129-38.
- [15] Akbal F. Adsorption of basic dyes from aqueous solution onto pumice powder. *Journal of colloid and interface science* 2005;286(2):455-8.
- [16] Yaghi OM, O'keeffe M, Ockwig NW, Chae HK, Eddaoudi M, Kim J. Reticular synthesis and the design of new materials. *Nature* 2003;423(6941):705.
- [17] Yaghi OM, Li H, Davis C, Richardson D, Groy TL. Synthetic Strategies, Structure Patterns, and Emerging Properties in the Chemistry of Modular Porous Solids. *Accounts of Chemical Research* 1998;31(8):474-84.
- [18] Batten SR, Robson R. Interpenetrating nets: ordered, periodic entanglement. *Angewandte Chemie International Edition* 1998;37(11):1460-94.
- [19] Férey G. Building units design and scale chemistry. *Journal of Solid State Chemistry* 2000;152(1):37-48.
- [20] Kitagawa S, Kondo M. Functional micropore chemistry of crystalline metal complex-assembled compounds. *Bulletin of the Chemical Society of Japan* 1998;71(8):1739-53.
- [21] Yaghi O, O'Keeffe M, Kanatzidis M. Design of solids from molecular building blocks: golden opportunities for solid state chemistry. *Journal of Solid State Chemistry* 2000;152(1):1-2.
- [22] Furukawa H, Cordova KE, O'Keeffe M, Yaghi OM. The chemistry and applications of metal-organic frameworks. *Science* 2013;341(6149):1230444.
- [23] Zhou H-C, Long JR, Yaghi OM. Introduction to metal-organic frameworks. ACS Publications; 2012.
- [24] Mueller U, Schubert M, Teich F, Puetter H, Schierle-Arndt K, Pastre J. Metal-organic frameworks-prospective industrial applications. *Journal of Materials Chemistry* 2006;16(7):626-36.
- [25] Jacoby M. Heading to market with MOFs. *Chem Eng News* 2008;86(34):13-6.
- [26] Furukawa H, Ko N, Go YB, Aratani N, Choi SB, Choi E, et al. Ultrahigh porosity in metal-organic frameworks. *Science* 2010;329(5990):424-8.
- [27] Millward AR, Yaghi OM. Metal-organic frameworks with exceptionally high capacity for storage of carbon dioxide at room temperature. *Journal of the American Chemical Society* 2005;127(51):17998-9.
- [28] Caskey SR, Wong-Foy AG, Matzger AJ. Dramatic tuning of carbon dioxide uptake via metal substitution in a coordination polymer with cylindrical pores. *Journal of the American Chemical Society* 2008;130(33):10870-1.
- [29] Hamon L, Serre C, Devic T, Loiseau T, Millange F, Férey G, et al. Comparative study of hydrogen sulfide adsorption in the MIL-53 (Al, Cr, Fe), MIL-47 (V), MIL-100 (Cr), and MIL-101 (Cr) metal-organic frameworks at room temperature. *Journal of the American Chemical Society* 2009;131(25):8775-7.
- [30] Karra JR, Walton KS. Effect of open metal sites on adsorption of polar and nonpolar molecules in metal-organic framework Cu-BTC. *Langmuir* 2008;24(16):8620-6.
- [31] Blanco-Brieva G, Campos-Martin JM, Al-Zahrani S, Fierro JL. Effectiveness of metal-organic frameworks for removal of refractory organo-sulfur compound present in liquid fuels. *Fuel* 2011;90(1):190-7.
- [32] Arstad B, Fjellvåg H, Kongshaug KO, Swang O, Blom R. Amine functionalised metal organic frameworks (MOFs) as adsorbents for carbon dioxide. *Adsorption* 2008;14(6):755-62.
- [33] Haque E, Lee JE, Jang IT, Hwang YK, Chang J-S, Jegal J, et al. Adsorptive removal of methyl orange from aqueous solution with metal-organic frameworks, porous chromium-benzenedicarboxylates. *Journal of Hazardous Materials* 2010;181(1):535-42.
- [34] Peterson GW, Wagner GW, Balboa A, Mahle J, Sewell T, Karwacki CJ. Ammonia vapor removal by Cu₃(BTC)₂ and its characterization by MAS NMR. *The Journal of Physical Chemistry C* 2009;113(31):13906-17.

- [35] Khan NA, Jhung SH. Adsorptive removal of benzothio-
phene using porous copper-benzenetricarboxylate
loaded with phosphotungstic acid. *Fuel Processing
Technology* 2012;100:49-54.
- [36] Khan NA, Hasan Z, Jhung SH. Adsorptive removal of
hazardous materials using metal-organic frameworks
(MOFs): A review. *Journal of Hazardous Materials*
2013;244-245:444-56.
- [37] Khan NA, Jun JW, Jeong JH, Jhung SH. Remarkable
adsorptive performance of a metal-organic framework,
vanadium-benzenedicarboxylate (MIL-47), for
benzothio-
phene. *Chemical Communications* 2011;47
(4):1306-8.
- [38] Ahmed I, Hasan Z, Khan NA, Jhung SH. Adsorptive
denitrogenation of model fuels with porous
metal-organic frameworks (MOFs): Effect of acidity
and basicity of MOFs. *Applied Catalysis B:
Environmental* 2013;129:123-9.
- [39] Khan NA, Jhung SH. Low-temperature loading of Cu⁺
species over porous metal-organic frameworks
(MOFs) and adsorptive desulfurization with Cu⁺-
loaded MOFs. *Journal of Hazardous Materials*
2012;237-238:180-5.
- [40] Britt D, Tranchemontagne D, Yaghi OM. Metal-organic
frameworks with high capacity and
selectivity for harmful gases. *Proceedings of the
National Academy of Sciences* 2008;105(33):11623-7.
- [41] Hamon L, Leclerc H, Ghoufi A, Oliviero L, Travert A,
Lavalley J-C, et al. Molecular insight into the
adsorption of H₂S in the flexible MIL-53 (Cr) and
rigid MIL-47 (V) MOFs: infrared spectroscopy
combined to molecular simulations. *The Journal of
Physical Chemistry C* 2011;115(5):2047-56.
- [42] Mo Z-W, Zhou H-L, Zhou D-D, Lin R-B, Liao P-Q, He
C-T, et al. Mesoporous Metal-Organic Frameworks
with Exceptionally High Working Capacities for
Adsorption Heat Transformation. *Advanced Materials*
2018;30(4):1704350.
- [43] Xue H, Huang X-S, Yin Q, Hu X-J, Zheng H-Q, Huang
G, et al. Bimetallic Cationic Metal-Organic
Frameworks for Selective Dye Adsorption and Effective
Cr₂O₇²⁻ Removal. *Crystal Growth & Design* 2020;20
(8):4861-6.
- [44] Azhar MR, Abid HR, Periasamy V, Sun H, Tade MO,
Wang S. Adsorptive removal of antibiotic sulfonamide
by UiO-66 and ZIF-67 for wastewater treatment.
Journal of Colloid and Interface Science 2017;500:
88-95.
- [45] Al Amery N, Abid HR, Wang S, Liu S. Enhancing
Acidic Dye Adsorption by Updated Version of UiO-66.
Journal of Applied Materials and Technology 2020;1
(2):54-62.
- [46] Abid HR, Pham GH, Ang H-M, Tade MO, Wang S.
Adsorption of CH₄ and CO₂ on Zr-metal organic
frameworks. *Journal of Colloid and Interface Science*
2012;366(1):120-4.
- [47] Hameed BH, Ahmad AA. Batch adsorption of
methylene blue from aqueous solution by garlic peel,
an agricultural waste biomass. *Journal of Hazardous
Materials* 2009;164(2):870-5.
- [48] Hameed B, Rahman A. Removal of phenol from
aqueous solutions by adsorption onto activated carbon
prepared from biomass material. *Journal of Hazardous
Materials* 2008;160(2):576-81.
- [49] Ho Y-S, McKay G. Pseudo-second order model for
sorption processes. *Process biochemistry* 1999;34
(5):451-65.
- [50] Wang S, Li H, Xu L. Application of zeolite MCM-22 for
basic dye removal from wastewater. *Journal of colloid
and interface science* 2006;295(1):71-8.
- [51] Weber WJ, Morris JC. Kinetics of adsorption on carbon
from solution. *Journal of the Sanitary Engineering
Division* 1963;89(2):31-60.
- [52] Gupta N, Kushwaha AK, Chattopadhyaya MC.
Application of potato (*Solanum tuberosum*) plant
wastes for the removal of methylene blue and malachite
green dye from aqueous solution. *Arabian Journal of
Chemistry* 2016;9:S707-S16.
- [53] Lin S-H, Juang R-S. Adsorption of phenol and its
derivatives from water using synthetic resins and
low-cost natural adsorbents: a review. *Journal of
environmental management* 2009;90(3):1336-49.
- [54] Uddin MT, Islam MA, Mahmud S, Rukanuzzaman M.
Adsorptive removal of methylene blue by tea waste.
Journal of Hazardous Materials 2009;164(1):53-60.
- [55] Lagergren S. Zur theorie der sogenannten adsorption
gelöster stoffe, *Kungliga Svenska
Vetenskapsakademiens. Handlingar.* 24 (4), 1-39.
*Microchemical Journal Environ Sci Technol J Colloid
Interface Sci J Colloid Interface Sci Environ Sci
Technol Rev Soc Quím Perú, American Water Works
Association Chem Eng J* 1898.
- [56] Ho YS, McKay G. Pseudo-second order model for
sorption processes. *Process Biochemistry* 1999;34
(5):451-65.
- [57] Demir H, Top A, Balköse D, Ülkü S. Dye adsorption
behavior of *Luffa cylindrica* fibers. *Journal of
Hazardous Materials* 2008;153(1-2):389-94.
- [58] Rattanaphani S, Chairat M, Bremner JB, Rattanaphani
V. An adsorption and thermodynamic study of lac
dyeing on cotton pretreated with chitosan. *Dyes and
pigments* 2007;72(1):88-96.
- [59] Moussavi G, Khosravi R. The removal of cationic dyes
from aqueous solutions by adsorption onto pistachio
hull waste. *Chemical Engineering Research and Design*
2011;89(10):2182-9.
- [60] Namasivayam C, Sumithra S. Removal of direct red
12B and methylene blue from water by adsorption onto
Fe (III)/Cr (III) hydroxide, an industrial solid waste.
Journal of Environmental Management 2005;74
(3):207-15.
- [61] Gupta G, Prasad G, Panday K, Singh V. Removal of
chrome dye from aqueous solutions by fly ash. *Water,
Air, and Soil Pollution* 1988;37(1-2):13-24.
- [62] Hameed BH, Ahmad AL, Latiff KNA. Adsorption of
basic dye (methylene blue) onto activated carbon
prepared from rattan sawdust. *Dyes and Pigments*
2007;75(1):143-9.
- [63] Hameed BH, Din ATM, Ahmad AL. Adsorption of
methylene blue onto bamboo-based activated carbon:

- Kinetics and equilibrium studies. *Journal of Hazardous Materials* 2007;141(3):819-25.
- [64] Hall KR, Eagleton LC, Acrivos A, Vermeulen T. Pore-and solid-diffusion kinetics in fixed-bed adsorption under constant-pattern conditions. *Industrial & Engineering Chemistry Fundamentals* 1966;5(2):212-23.
- [65] Gupta GS, Prasad G, Panday KK, Singh VN. Removal of chrome dye from aqueous solutions by fly ash. *Water, Air, and Soil Pollution* 1988;37(1):13-24.
- [66] Kumar KV, Ramamurthi V, Sivanesan S. Modeling the mechanism involved during the sorption of methylene blue onto fly ash. *Journal of colloid and interface science* 2005;284(1):14-21.
- [67] Abid HR, Ang HM, Wang S. Effects of ammonium hydroxide on the structure and gas adsorption of nanosized Zr-MOFs (UiO-66). *Nanoscale* 2012;4(10):3089-94.
- [68] Rada ZH, Abid HR, Sun H, Wang S. Bifunctionalized Metal Organic Frameworks, UiO-66-NO₂-N (N = -NH₂, -(OH)₂, -(COOH)₂), for Enhanced Adsorption and Selectivity of CO₂ and N₂. *Journal of Chemical & Engineering Data* 2015;60(7):2152-61.
- [69] Al Haydar M, Abid HR, Sunderland B, Wang S. Multimetal organic frameworks as drug carriers: aceclofenac as a drug candidate. *Drug Des Devel Ther* 2018;13:23-35.
- [70] Abid HR, Tian H, Ang H-M, Tade MO, Buckley CE, Wang S. Nanosize Zr-metal organic framework (UiO-66) for hydrogen and carbon dioxide storage. *Chemical Engineering Journal* 2012;187:415-20.
- [71] Abid HR, Shang J, Ang H-M, Wang S. Amino-functionalized Zr-MOF nanoparticles for adsorption of CO₂ and CH₄. *International Journal of Smart and Nano Materials* 2013;4(1):72-82.
- [72] Di Marino A, Mendicuti F. Thermodynamics of complexation of dimethyl esters of tere-, iso-, and phthalic acids with α - and β -cyclodextrins. *Applied spectroscopy* 2004;58(7):823-30.
- [73] Dhumal NR, Singh MP, Anderson JA, Kiefer J, Kim HJ. Molecular Interactions of a Cu-Based Metal-Organic Framework with a Confined Imidazolium-Based Ionic Liquid: A Combined Density Functional Theory and Experimental Vibrational Spectroscopy Study. *The Journal of Physical Chemistry C* 2016;120(6):3295-304.
- [74] Coates J. Interpretation of infrared spectra, a practical approach. *Encyclopedia of analytical chemistry* 2000;12:10815-37.
- [75] Aroke U, Abdulkarim A, Ogubunka R. Fourier-transform infrared characterization of kaolin, granite, bentonite and barite. *ATBU Journal of Environmental Technology* 2013;6(1):42-53.
- [76] Ho Y, McKay G. The kinetics of sorption of basic dyes from aqueous solution by sphagnum moss peat. *The Canadian Journal of Chemical Engineering* 1998;76(4):822-7.
- [77] Bulut Y, Aydın H. A kinetics and thermodynamics study of methylene blue adsorption on wheat shells. *Desalination* 2006;194(1-3):259-67.
- [78] Senthil Kumar P, Senthamarai C, Durgadevi A. Adsorption kinetics, mechanism, isotherm, and thermodynamic analysis of copper ions onto the surface modified agricultural waste. *Environmental Progress & Sustainable Energy* 2014;33(1):28-37.
- [79] Ai L, Jiang J. Fast removal of organic dyes from aqueous solutions by AC/ferrospinel composite. *Desalination* 2010;262(1):134-40.
- [80] Ai L, Zhang C, Chen Z. Removal of methylene blue from aqueous solution by a solvothermal-synthesized graphene/magnetite composite. *Journal of Hazardous Materials* 2011;192(3):1515-24.
- [81] Abid HR, Rada ZH, Li Y, Mohammed HA, Wang Y, Wang S, et al. Boosting CO₂ adsorption and selectivity in metal-organic frameworks of MIL-96(Al) via second metal Ca coordination. *RSC Advances* 2020;10(14):8130-9.
- [82] Doğan M, Özdemir Y, Alkan M. Adsorption kinetics and mechanism of cationic methyl violet and methylene blue dyes onto sepiolite. *Dyes and Pigments* 2007;75(3):701-13.
- [83] Zaboon S, Abid HR, Yao Z, Gubner R, Wang S, Barifcani A. Removal of monoethylene glycol from wastewater by using Zr-metal organic frameworks. *Journal of Colloid and Interface Science* 2018;523:75-85.
- [84] Ji B, Shao F, Hu G, Zheng S, Zhang Q, Xu Z. Adsorption of methyl tert-butyl ether (MTBE) from aqueous solution by porous polymeric adsorbents. *Journal of Hazardous Materials* 2009;161(1):81-7.
- [85] Gupta N, Kushwaha AK, Chattopadhyaya M. Adsorption studies of cationic dyes onto Ashoka (*Saraca asoca*) leaf powder. *Journal of the Taiwan Institute of Chemical Engineers* 2012;43(4):604-13.
- [86] Weng C-H, Lin Y-T, Tzeng T-W. Removal of methylene blue from aqueous solution by adsorption onto pineapple leaf powder. *Journal of Hazardous Materials* 2009;170(1):417-24.
- [87] Ho Y-S, McKay G. Sorption of dye from aqueous solution by peat. *Chemical engineering journal* 1998;70(2):115-24.
- [88] Ponnusami V, Vikram S, Srivastava SN. Guava (*Psidium guajava*) leaf powder: Novel adsorbent for removal of methylene blue from aqueous solutions. *Journal of Hazardous Materials* 2008;152(1):276-86.
- [89] Oliveira LS, Franca AS, Alves TM, Rocha SD. Evaluation of untreated coffee husks as potential biosorbents for treatment of dye contaminated waters. *Journal of Hazardous Materials* 2008;155(3):507-12.
- [90] Otero M, Rozada F, Calvo LF, García AI, Morán A. Kinetic and equilibrium modelling of the methylene blue removal from solution by adsorbent materials produced from sewage sludges. *Biochemical Engineering Journal* 2003;15(1):59-68.
- [91] Banat F, Al-Asheh S, Al-Makhadmeh L. Evaluation of the use of raw and activated date pits as potential adsorbents for dye containing waters. *Process Biochemistry* 2003;39(2):193-202.
- [92] Ghosh D, Bhattacharyya K. Removing colour from aqueous medium by sorption on natural clay: a study

- with methylene blue. *INDIAN JOURNAL OF ENVIRONMENTAL PROTECTION* 2001;21(10):903-10.
- [93] Yao Y, Xu F, Chen M, Xu Z, Zhu Z. Adsorption behavior of methylene blue on carbon nanotubes. *Bioresource Technology* 2010;101(9):3040-6.
- [94] Vadivelan V, Kumar KV. Equilibrium, kinetics, mechanism, and process design for the sorption of methylene blue onto rice husk. *Journal of Colloid and Interface Science* 2005;286(1):90-100.
- [95] Kumar KV, Porkodi K. Mass transfer, kinetics and equilibrium studies for the biosorption of methylene blue using *Paspalum notatum*. *Journal of Hazardous Materials* 2007;146(1):214-26.
- [96] Banerjee S, Dastidar MG. Use of jute processing wastes for treatment of wastewater contaminated with dye and other organics. *Bioresource Technology* 2005;96(17):1919-28.
- [97] Annadurai G, Juang R-S, Lee D-J. Use of cellulose-based wastes for adsorption of dyes from aqueous solutions. *Journal of Hazardous Materials* 2002;92(3):263-74.
- [98] Wang S, Boyjoo Y, Choueib A. A comparative study of dye removal using fly ash treated by different methods. *Chemosphere* 2005;60(10):1401-7.
- [99] Woolard CD, Strong J, Erasmus CR. Evaluation of the use of modified coal ash as a potential sorbent for organic waste streams. *Applied Geochemistry* 2002;17(8):1159-64.
- [100] Gürses A, Karaca S, Doğar Ç, Bayrak R, Açıkıldız M, Yalçın M. Determination of adsorptive properties of clay/water system: methylene blue sorption. *Journal of Colloid and Interface Science* 2004;269(2):310-4.



This article is licensed under a [Creative Commons Attribution 4.0 International License](https://creativecommons.org/licenses/by/4.0/).